A double pendulum fixed at the L1 libration point: a precursor to a Mars-Phobos space elevator

Vladimir S. Aslanov

Moscow Aviation Institute (National Research University), 4, Volokolamskoe Shosse, A-80, GSP-3, Moscow, Russia

+7-9276889791

aslanov_vs@mail.ru

http://aslanov.ssau.ru/

Abstract The paper is devoted to the investigation of the possibility of constructing a double pendulum fixed at the L1 libration point in the framework of the planar circular restricted three-body problem. Possible configurations of pendulum equilibrium positions depending on the ratios of masses and lengths of single pendulums composing the double pendulum are shown. The stability of two equilibrium positions is proved using Sylvester's criterion. In the first position, the pendulum is oriented toward a Moon, and it is oriented toward a Planet in the second position. Small motions near these stable equilibrium configurations are studied. The natural frequencies and mode ratios are obtained analytically and their dependence on the mass and length ratios of the pendulums is analyzed. The conducted studies demonstrate the possibility of building a space elevator in the Mars-Phobos system from the L1 libration point to a Moon (distance from the L1 point to the surface of Phobos ~3.4 km), or to a Planet (distance from the L1 point to the surface of Mars ~7800 km). This also opens up the opportunity of building a two-part space elevator from Mars to Phobos. The obtained natural frequencies and mode ratios allow us to predict in advance the possible motions of a space elevator under small perturbations relative to the stable equilibrium position.

Keywords *L1 libration point · Double pendulum · Equilibrium positions · Natural frequencies · Normal modes · Space elevator.*

1 Introduction

Space tethers can be used in many future space missions as an economical and simple alternative to propulsion systems. Several books [1–4] and hundreds of scientific articles (eg. [5–17]) have explored the possibilities of space tether systems, including studies of the distant planets of the solar system and its moons. One such promising mission is the Phobos L1 Operational Tether Experiment (PHLOTE), which will explore the surface of Phobos using a tether "anchored" at the L1 libration point of the Mars-Phobos system [16, 17], about 3.4 km from the surface of Phobos. The tether will be deployed from an orbiting spacecraft located at the L1 libration point in the direction of Phobos. Instruments placed in the tether's end mass will study the surface of Phobos from low altitude. The PHOLE mission can be improved by adding the tether system with a climber that moves from the tether's end mass (instrument package) to the spacecraft at the L1 point and back. When the climber is stopped, this tether system becomes a double pendulum. A PHLOTE-like mission in which the tether is a space elevator [18-22] as a three-body tether system with a moving climber could be an evolution of the PHLOTE mission. The three-body tether system is a double pendulum with variable tether lengths. The first step in studying this complex mechanical system is to consider the situation where the lengths of the pendulums do not change. As it was several decades ago [23, 24], the study of the behaviour of the double pendulum in various applications is still relevant today [25-38]. The double pendulum fixed at L1 libration point differs from the classical double pendulum in that there are two gravitational forces acting on it from the primary bodies and a centrifugal force according to the restricted three-body problem [39].

The goal of the paper is to study the behaviour of the double pendulum fixed at L1 libration point as a prototype of the space elevator connecting the surface of a moon with L1 libration point. The problem of the double pendulum fixed at the L1 libration point is presented for the first time, so it is important at the initial stage to understand the main features of the behaviour and to show the possibility of using the double pendulum for practical purposes in studying planetary moons. In principle, it does not matter whether it is an Earth-Moon or a Mars-Phobos pair of primary bodies. The most interesting of these is undoubtedly the L1 libration point of the Mars-Phobos system, which is less than 3.5 km from the surface of Phobos.

To achieve the stated goal, firstly, the basic assumptions in the framework of the circular planar restricted three-body problem are formulated and the motion equations of the double pendulum in the rotating Cartesian coordinate system are derived in polar coordinates with respect to L1 libration point using the Lagrange formalism. Furthermore, using the Sylvester criterion, it is shown that the upper position (in the direction of a Planet (primary 1)) and the lower position (in the direction of a Moon (primary 2)) of the double pendulum are stable. Secondly, the equilibrium positions of the resulting nonlinear equations of motion are plotted for different mass ratios and lengths of the pendulums. Thirdly, eigenfrequencies and ratio modes are found for small motions around equilibrium configurations near the upper and lower equilibrium positions of the double pendulum. Finally, conclusions are drawn about the possibility of constructing a space elevator based on the studies carried out on the double pendulum as a three-body system.

2 Motion equations of a double pendulum fixed at the L1 libration point

In this section the equations of plane motion of a double pendulum in two gravitational fields of two primaries (Planet-Moon) in rotating polar coordinates with respect to the L1 libration point are derived using the Lagrange formalism in the framework of the circular restricted three-body problem [39].

2.1 Key assumptions

The following acceptable assumptions are introduced:

1. It is supposed that the primaries move in circular orbits around their mutual mass center (point O in Fig. 1).

2. The end masses of the pendulums m_1 and m_2 are significantly smaller than the primary masses M_1 and M_2

$$m_1,\, m_2 \ll M_2 < M_1 \tag{1}$$

3. The pendulums consist of weightless rigid rods

$$l_1, l_2 = const \tag{2}$$

where l_1, l_2 are the pendulum lengths (Fig. 1).

4. In the circular restricted three-body problem, the mean rotation is

$$n = \frac{df}{dt} = const \tag{3}$$

where f is the true anomaly.

5. In all considered cases, only in-plane motion is studied.

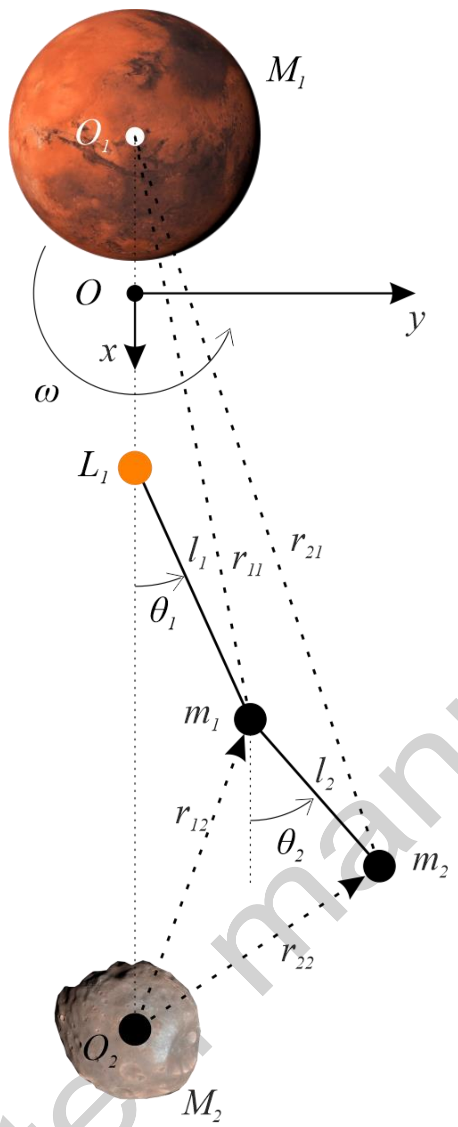

Fig. 1 The frame Oxy

2.2 Motion equations of a double pendulum fixed at the L1 libration point

We use the Lagrangian formalism to write the planar motion equations of a double pendulum in the Local-Vertical-Local-Horizontal frame Oxy within the scope of the classical restricted three-body problem [39]

$$\frac{d}{dt}\frac{\partial L}{\partial \dot{\theta}_i} - \frac{\partial L}{\partial \theta_i} = 0\,, \qquad (i = 1, 2) \tag{4}$$

where L is the Lagrangian, $\boldsymbol{\theta} = (\theta_1, \theta_2)^T$ is the vector of generalized coordinates (Fig.1). The positions of the L1 libration point and the two end masses (m_1, m_2) of the pendulums can be written in generalized coordinates as

$$\mathbf{r}_{L_1} = (a, 0, 0)^T, \tag{5}$$

$$\mathbf{r}_1 = (a + l_1 \cos\theta_1, l_1 \sin\theta_1, 0)^T, \tag{6}$$

$$\mathbf{r}_2 = (a + l_1 \cos\theta_1 + l_2 \cos\theta_2, l_1 \sin\theta_1 + l_2 \sin\theta_2, 0)^T \tag{7}$$

where a is the coordinate of the L_1 libration point in the frame Oxy. The velocities of the end masses are defined in the inertial coordinate system as the sum of derivatives of vectors (6) и (7) and velocity due to rotation of the frame Oxy

$$\mathbf{V}_1 = \frac{d\mathbf{r}_1}{dt} + \boldsymbol{\omega} \times \mathbf{r}_1, \qquad \mathbf{V}_2 = \frac{d\mathbf{r}_2}{dt} + \boldsymbol{\omega} \times \mathbf{r}_2 \tag{8}$$

where $\boldsymbol{\omega} = (0, 0, n)^T$ is the vector of the angular velocity of the frame Oxy. The Lagrangian is defined as the sum of kinetic and potential energy

$$L = T - V \tag{9}$$

The kinetic and potential energy are given by

$$T = \frac{m_1}{2}\mathbf{V}_1 \cdot \mathbf{V}_1 + \frac{m_2}{2}\mathbf{V}_2 \cdot \mathbf{V}_2, \tag{10}$$

$$V = Gm_1\left(\frac{M_1}{\sqrt{\mathbf{r}_{11} \cdot \mathbf{r}_{11}}} + \frac{M_2}{\sqrt{\mathbf{r}_{12} \cdot \mathbf{r}_{12}}}\right) + Gm_2\left(\frac{M_1}{\sqrt{\mathbf{r}_{21} \cdot \mathbf{r}_{21}}} + \frac{M_2}{\sqrt{\mathbf{r}_{22} \cdot \mathbf{r}_{22}}}\right) \tag{11}$$

where G is the gravitational constant,

$$\mathbf{r}_{11} = \mathbf{r}_1 - \mathbf{R}_1, \quad \mathbf{r}_{12} = \mathbf{r}_1 - \mathbf{R}_2, \quad \mathbf{r}_{21} = \mathbf{r}_2 - \mathbf{R}_1, \quad \mathbf{r}_{22} = \mathbf{r}_2 - \mathbf{R}_2 \tag{12}$$

The coordinates of the primaries O_1 and O_2 in the frame Oxy respectively are

$$\mathbf{R}_1 = (-\mu p, 0, 0)^T, \qquad \mathbf{R}_2 = ((1-\mu)p, 0, 0)^T \tag{13}$$

where p is the distance between the primaries, $\mu = \dfrac{M_2}{M_1 + M_2}$ is the mass ratio, M_1 and M_2 are masses of the primaries 1 and 2, respectively.

Considering Eqs. (12) and (13), the kinetic energy (10) is given by the following equation

$$T = \frac{m}{2(1+\sigma)(1+\lambda)^2}[l^2 \sin^2\theta_1\left(n + \dot{\theta}_1\right)^2 + \left(n\left(a + a\lambda + l\cos\theta_1\right) + l\cos\theta_1\dot{\theta}_1\right)^2 +$$

$$\sigma(\left(n\left(a + a\lambda + l\cos\theta_1 + l\lambda\cos\theta_2\right) + l\dot{\theta}_1\cos\theta_1 + l\lambda\dot{\theta}_2\cos\theta_2\right)^2 +$$

$$l^2\left(n\left(\sin\theta_1 + \lambda\sin\theta_2\right) + \dot{\theta}_1\sin\theta_1 + \lambda\dot{\theta}_2\sin\theta_2\right)^2)] \tag{14}$$

where

$$\lambda = \frac{l_2}{l_1}, \; \sigma = \frac{m_2}{m_1}, \; l = l_1 + l_2, \; m = m_1 + m_2 \tag{15}$$

Similarly the potential energy can be written down in the following form

$$V = \frac{G\,m}{(1+\sigma)}\left[\frac{M_1}{r_{11}} + \frac{M_2}{r_{12}} + \sigma\left(\frac{M_1}{r_{21}} + \frac{M_2}{r_{22}}\right)\right] \tag{16}$$

where

$$r_{11} = \sqrt{\rho_1{}^2 + 2\rho_1 l_1 \cos\theta_1 + l_1^2} = \sqrt{\left(\rho_1 + \frac{l\cos\theta_1}{1+\lambda}\right)^2 + \frac{l^2\sin^2\theta_1}{(1+\lambda)^2}}\ , \tag{17}$$

$$r_{12} = \sqrt{\rho_2{}^2 + 2\rho_2 l_1 \cos\theta_1 + l_1^2} = \sqrt{\left(\rho_2 + \frac{l\cos\theta_1}{1+\lambda}\right)^2 + \frac{l^2\sin^2\theta_1}{(1+\lambda)^2}}\ , \tag{18}$$

$$r_{21} = \sqrt{(\rho_1 + l_1\cos\theta_1 + l_2\cos\theta_2)^2 + (l_1\sin\theta_1 + l_2\sin\theta_2)^2} =$$
$$\frac{1}{1+\lambda}\sqrt{\left((1+\lambda)\rho_1 + l\cos\theta_1 + l\lambda\cos\theta_2\right)^2 + \left(l\sin\theta_1 + l\lambda\sin\theta_2\right)^2}\ , \tag{19}$$

$$r_{22} = \sqrt{(\rho_2 + l_1\cos\theta_1 + l_2\cos\theta_2)^2 + (l_1\sin\theta_1 + l_2\sin\theta_2)^2} =$$
$$\frac{1}{1+\lambda}\sqrt{\left((1+\lambda)\rho_2 + l\cos\theta_1 + l\lambda\cos\theta_2\right)^2 + \left(l\sin\theta_1 + l\lambda\sin\theta_2\right)^2}\ , \tag{20}$$

$$\rho_1 = a + p\mu,\ \ \rho_2 = a - p(1-\mu) \tag{21}$$

The equations of the double pendulum (4) can be written in terms of Eqs. (14)-(21) as follows

$$\frac{1}{1+\lambda} l(2n\lambda\sigma\dot{\theta}_2\sin\theta_{12} + \lambda\sigma(n^2 + \dot{\theta}_2{}^2)\sin\theta_{12} + (1+\sigma)\ddot{\theta}_1 + \lambda\sigma\cos\theta_{12}\ddot{\theta}_2) +$$
$$an^2(1+\sigma)\sin\theta_1 - GM_1\left(\frac{\sin\theta_1\rho_1}{r_{11}^{3/2}} + \frac{\sigma\left(\frac{\lambda}{1+\lambda} l\sin\theta_{12} + \rho_1\sin\theta_1\right)}{r_{21}^{3/2}}\right) -$$
$$GM_2\left(\frac{\rho_2\sin\theta_1}{r_{12}^{3/2}} + \frac{\sigma\left(\frac{\lambda}{1+\lambda} l\sin\theta_{12} + \rho_2\sin\theta_1\right)}{r_{22}^{3/2}}\right) = 0, \tag{22}$$

$$\frac{l}{1+\lambda}(-2n\dot{\theta}_1\sin\theta_{12} - \dot{\theta}_1{}^2\sin\theta_{12} + \cos\theta_{12}\ddot{\theta}_1 + \lambda\ddot{\theta}_2) +$$
$$\sin\theta_2\left(an^2 - G\left(\frac{M_1\rho_1}{r_{21}^{3/2}} + \frac{M_2\rho_2}{r_{22}^{3/2}}\right)\right) + \frac{l}{1+\lambda}\sin\theta_{12}\left(-n^2 + G\left(\frac{M_1}{r_{21}^{3/2}} + \frac{M_2}{r_{22}^{3/2}}\right)\right) = 0 \tag{23}$$

where $\theta_{12} = \theta_1 - \theta_2$.

2.3 Total potential energy

To find the equilibrium positions of the conservative system (21)-(22), we use the method proposed by Hertz [40, pp. 223-229]. The motion of the conservative system (21)-(22), which does not depend on the corresponding coordinate, is interpreted as a concealed cyclic motion, which, in fact, agrees with the formalism of Routh [41, p. 60]. The kinetic energy T depends on the mean rotation $n = \frac{df}{dt}$ and not on the true anomaly f according to Eq. (14), so the true anomaly is the concealed cyclical coordinate. This allows to represent the kinetic energy T as a sum of two terms, one τ of which depends on velocities $\dot{\theta}_1$ and $\dot{\theta}_2$, and the other T^* is the energy of concealed motions, which does not depend on the generalized velocities $\dot{\theta}_1$ and $\dot{\theta}_2$, but includes the factor n^2 :

$$T = T^* + \tau \tag{24}$$

where

$$T^* = \frac{m}{2(1+\sigma)(1+\lambda)^2} n^2[(a + a\lambda + l\cos\theta_1)^2 + l^2 \sin^2\theta_1 +$$
$$\sigma\left((a + a\lambda + l\cos\theta_1 + l\lambda\cos\theta_2)^2 + l^2(\sin\theta_1 + \lambda\sin\theta_2)^2\right)], \tag{25}$$

$$\tau = \frac{ml}{2(1+\sigma)(1+\lambda)^2}[l(1+\sigma)\dot{\theta}_1^2 + \lambda\sigma\dot{\theta}_2\left(2n\left(l\lambda + l\cos\theta_{12} + a(1+\lambda)\cos\theta_2\right) + l\lambda\dot{\theta}_2\right) +$$
$$2\dot{\theta}_1\left(an(1+\lambda)(1+\sigma)\cos\theta_1 + ln(1+\sigma+\lambda\sigma\cos\theta_{12}) + l\lambda\sigma\dot{\theta}_2\cos\theta_{12}\right)] \tag{26}$$

The potential energy extended by the kinetic energy of the concealed motions is called the total potential energy

$$\nu = V + T^* \tag{27}$$

Since part of the kinetic energy T^* does not depend on generalized velocities, it will not contribute to the first term of equation (4), and it can be formally attributed to potential energy. In this case, the potential energy takes the form (27), and the Lagrange equations written for the kinetic energy τ and potential energy ν will coincide with the equations of the original system. It is clear that the total energy of the conservative system (22)-(23) is conserved, taking into account Eqs. (24) и (27)

$$E = T + V = \tau + \nu = const \tag{28}$$

Fig. 2 shows $\nu - \nu_0$ [$\nu_0 = \nu(0,0)$] as a function of the coordinates θ_1, θ_2 for the equal pendulum $\lambda = 1$ ($l_1 = l_2 = 1700m$), $\sigma = 1$ ($m_1 = m_2 = 50kg$) fixed at the L1 libration point of the Mars-Phobos system. In the following, all numerical simulations are performed for the Mars-Phobos system as a Planet-Moon system (primaries).

As can be seen from Figs. 1 and 2, two cases correspond to the pendulum's stable equilibrium position:

1. The pendulum is directed to the small primary 2 (Phobos)

$$\theta_1 = 0, \theta_2 = 0 \tag{29}$$

2. The pendulum is directed to the large primary 1 (Mars)

$$\theta_1 = \pi, \theta_2 = \pi \tag{30}$$

The positions $\theta_1 = \pm\pi,\ \theta_2 = \pm\pi$ represent the physical position of the pendulum (30). The unstable equilibrium positions are:

1. $\theta_1 = 0,\ \theta_2 = \pm\pi$
2. $\theta_1 = \pm\pi,\ \theta_2 = 0$

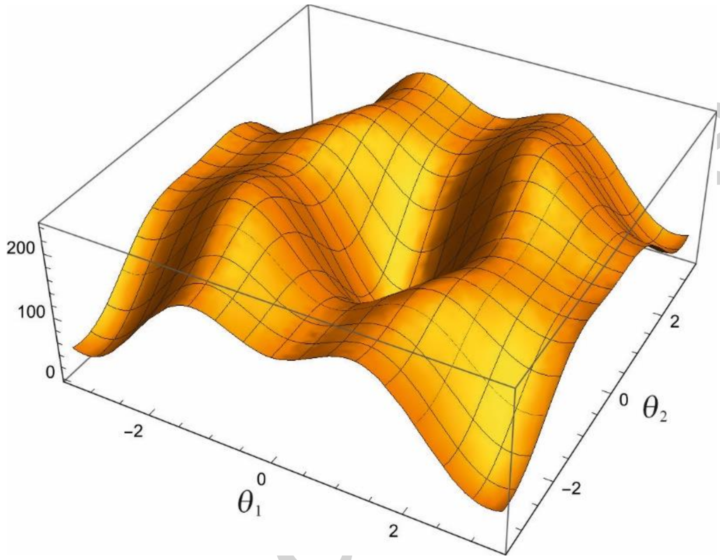

Fig. 2 Surface θ_1 - θ_2 -$(v - v_0)$ corresponds to the case of the equal pendulum $\lambda = 1,\ \sigma = 1$

2.4 Application of the Sylvester criterion to analyze the stability of the lower $\theta_1, \theta_2 = 0$ and upper $\theta_1, \theta_2 = \pi$ pendulum positions

According to Lagrange's theorem, if the potential energy of a conservative system has a minimum in the equilibrium position, then that equilibrium position is stable [42]. In applications of this theorem, it is most convenient to expand the total potential energy v in a series of powers of θ_1, θ_2, and use Sylvester's criterion. For a symmetric matrix

$$A = \begin{bmatrix} \dfrac{\partial^2 v}{\partial \theta_1^{\,2}} & \dfrac{\partial^2 v}{\partial \theta_1 \partial \theta_2} \\ \dfrac{\partial^2 v}{\partial \theta_2 \partial \theta_1} & \dfrac{\partial^2 v}{\partial \theta_2^{\,2}} \end{bmatrix} \tag{31}$$

8

the principal minors calculated in the equilibrium positions $\theta_1, \theta_2 = 0$ and $\theta_1, \theta_2 = \pi$ should be positive

$$\Delta_1^v = \left(\frac{\partial^2 v}{\partial \theta_1^2} \right) > 0 \qquad \Delta_2^v = \left(\frac{\partial^2 v}{\partial \theta_1^2} \frac{\partial^2 v}{\partial \theta_2^2} - \frac{\partial^2 v}{\partial \theta_1 \partial \theta_2} \frac{\partial^2 v}{\partial \theta_2 \partial \theta_1} \right) > 0 \tag{32}$$

If conditions (32) are satisfied, then the quadratic part of the potential energy is a positive definite quadratic form with respect to θ_1, θ_2, and the potential energy v is positive definite in a neighborhood of zero. Thus, the potential energy is an isolated minimum, and according to Lagrange's theorem, at the equilibrium position is stable. The principal minors (32) are calculated by differentiating the total potential energy (27) by means the symbolic programming language MATHEMATICA [43]. These equations are used in the construction of Fig. 3 and are not given here due to their rather cumbersome form. Fig. 3 shows that the principal minors (32) calculated at the points $\theta_1, \theta_2 = 0$ and $\theta_1, \theta_2 = \pi$ are positive for every $\lambda, \sigma \in (0.01, 10.0)$.

a

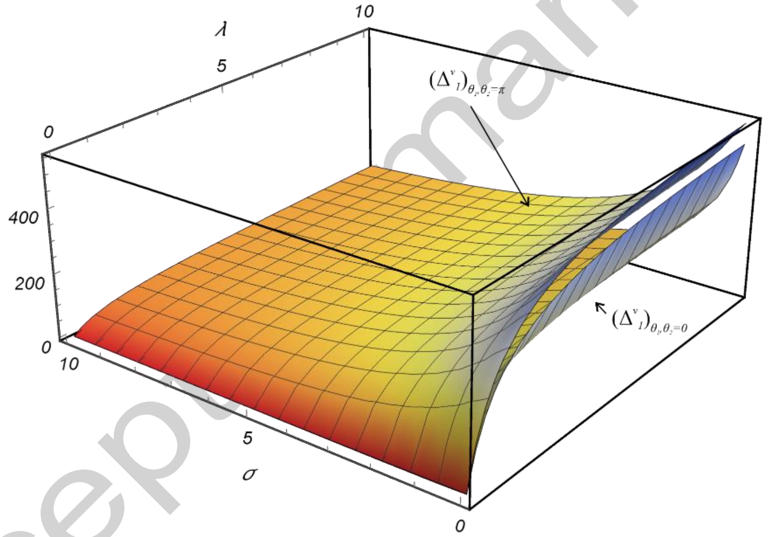

b

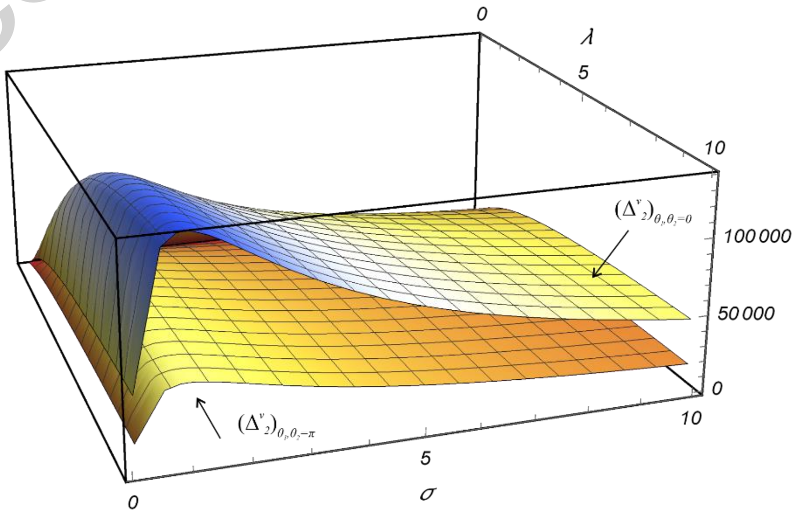

Fig. 3 a Surfaces λ - σ - $\left(\Delta_1^{\nu}\right)_{\theta_1,\theta_2=0}$ and λ - σ - $\left(\Delta_1^{\nu}\right)_{\theta_1,\theta_2=\pi}$; **b** Surfaces λ - σ - $\left(\Delta_2^{\nu}\right)_{\theta_1,\theta_2=0}$ and λ - σ - $\left(\Delta_2^{\nu}\right)_{\theta_1,\theta_2=\pi}$ correspond to the case of equal pendulum for $m=100kg$, $l=3400m$

3 Equilibrium positions map

In this section, the equilibrium positions of the double pendulum are considered. To determine the equilibrium configuration, velocity and acceleration in Eqs. (22) -(23) are put to zero

$$\dot{\theta}_1=0,\ \dot{\theta}_2=0, \qquad \ddot{\theta}_1=0,\ \ddot{\theta}_2=0 \tag{33}$$

and as a result, one obtains two nonlinear equations

$$F_1(\theta_1,\theta_2)=n^2((1+\sigma)a\sin\theta_1+\frac{\lambda\sigma}{1+\lambda}l\sin\theta_{12})-GM_1(\frac{\rho_1}{r_{11}^{3/2}}\sin\theta_1+\frac{\sigma}{r_{21}^{3/2}}(\frac{\lambda}{1+\lambda}l\sin\theta_{12}+\rho_1\sin\theta_1))-$$

$$GM_2(\frac{\rho_2}{r_{12}^{3/2}}\sin\theta_1+\frac{\sigma}{r_{22}^{3/2}}(\frac{\lambda}{1+\lambda}l\sin\theta_{12}+\rho_2\sin\theta_1))=0, \tag{34}$$

$$F_2(\theta_1,\theta_2)=n^2(a\sin\theta_2-\frac{l}{1+\lambda}\sin\theta_{12})+\frac{GM_1}{r_{21}^{3/2}}(-\rho_1\sin\theta_2+\frac{l}{1+\lambda}\sin\theta_{12})+$$

$$\frac{GM_2}{r_{22}^{3/2}}(-\rho_2\sin\theta_2+\frac{l}{1+\lambda}\sin\theta_{12})=0 \tag{35}$$

The equilibrium positions $\theta_1=\theta_{10}$ and $\theta_2=\theta_{20}$ are the roots of these equations, whose values depend on the ratio of masses σ and the ratio of pendulum lengths λ. Fig. 4 shows the maps of the equilibrium positions in the boundaries $-\pi\le\theta_1\le\pi, -\pi\le\theta_2\le\pi$ for 6 different values of σ and λ. The dotted and solid lines correspond to Eqs. (34) and (35), respectively. The intersection points of these lines are the equilibrium positions. Stable equilibrium positions are shown in the Fig. 4 with white points, and unstable positions are depicted with black points. The configuration of equilibrium positions varies depending on the values of the ratio of masses σ and pendulum lengths λ. Only the center point $\theta_1,\theta_2=(0,0)$ and the vertices $\theta_1,\theta_2=(\pm\pi,\pm\pi)$ keep their positions in all 6 cases.

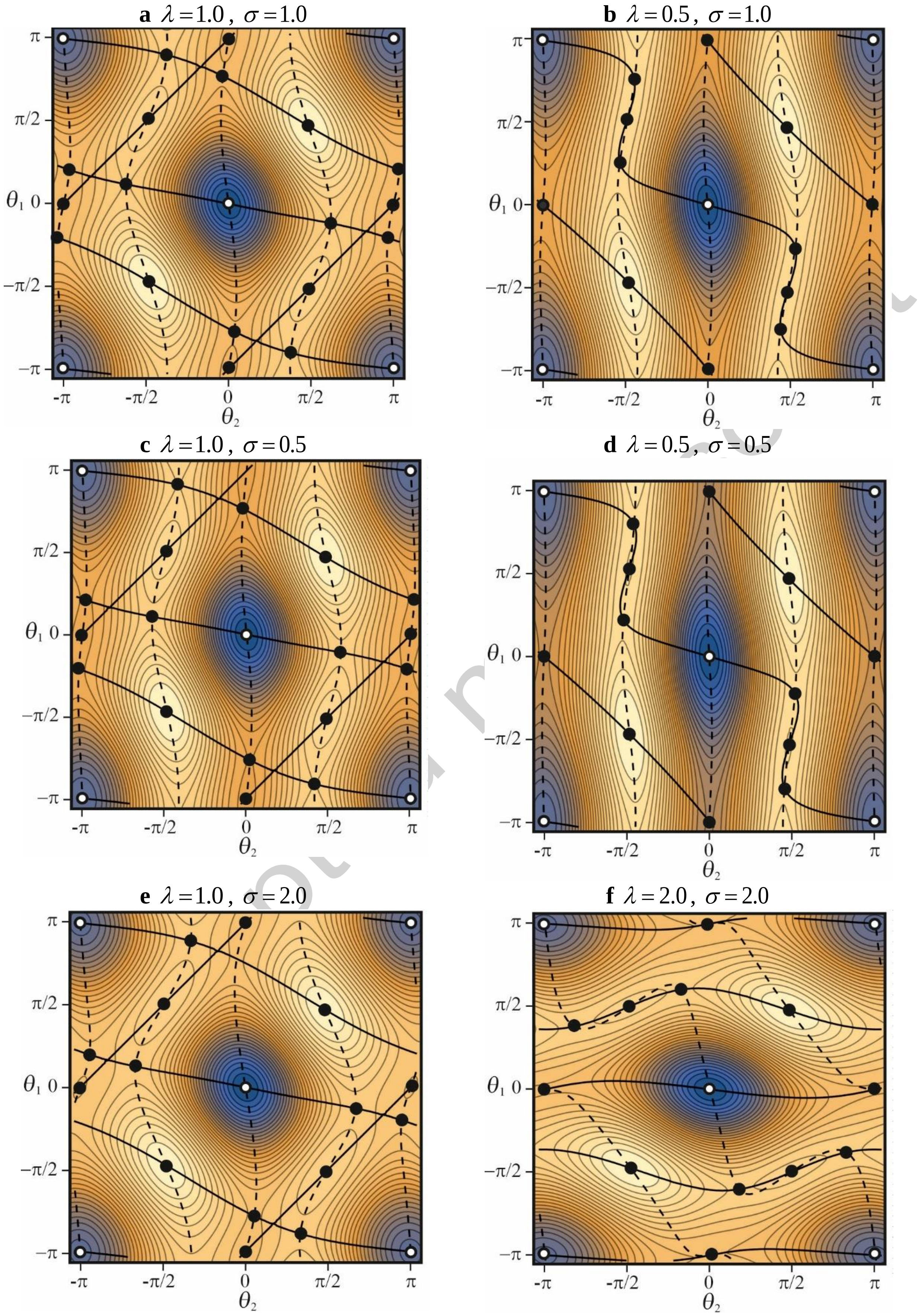

Fig. 4 Equilibrium position maps and the projection of total potential energy $(\nu - \nu_0)$ onto the θ_1, θ_2 - plane

Figs. 5a and 5b show the equilibrium lines as intersections of the surfaces defined by equations Eqs. (34) and (35) when one of the parameters (σ or λ) is fixed and the other is varied.

a $\sigma = 1.0$, $\lambda \in [0.4, 2.1]$ **b** $\lambda = 1.0$, $\sigma \in [0.4, 2.1]$

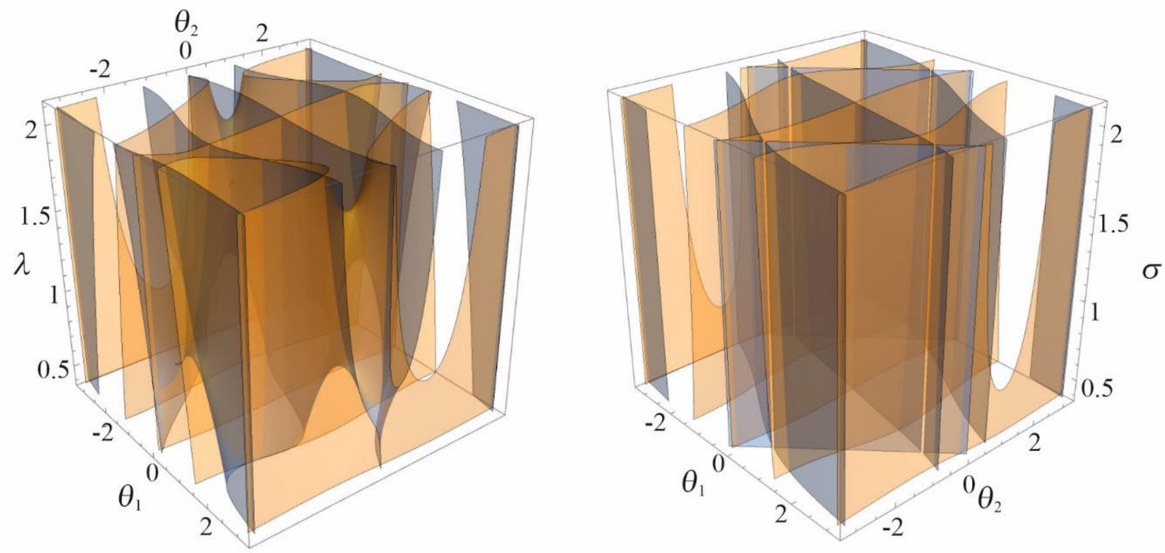

Fig. 5 Equilibrium position maps and the projection of total potential energy $(v - v_0)$ onto the θ_1, θ_2 - plane

4 Small motions around equilibrium configurations

Unlike the classical double pendulum in the Earth's gravitational field, which has only one stable equilibrium position, the double pendulum under the action of two gravitational forces and a centrifugal force directed toward the small primary 2 is considered. And as a result of the action of these forces, there are two stable equilibrium positions of the double pendulum, as shown in Section 2.4:

$$\theta_1 = 0, \theta_2 = 0, \quad \theta_1 = \pi, \theta_2 = \pi \tag{36}$$

We examine successive small motions near these two stable equilibrium positions.

4.1 Small motion around equilibrium configuration $\theta_1 = 0, \theta_2 = 0$

For small angles θ_1, θ_2 the linearization of Lagrange Eq. (4) results in

$$\begin{pmatrix} \ddot{\theta}_1 \\ \ddot{\theta}_2 \end{pmatrix} = \begin{pmatrix} c_{11} & c_{12} \\ c_{21} & c_{22} \end{pmatrix} \begin{pmatrix} \theta_1 \\ \theta_2 \end{pmatrix} \tag{37}$$

where

$$c_{11} = \frac{1+\lambda}{l}[-n^2(a-\sigma(a+l)) + GM_1(\frac{\rho_1}{R_{11}^3} + \frac{\sigma}{R_{21}^2}) + GM_2(\frac{\rho_2}{R_{12}^3} - \frac{\sigma}{R_{22}^2})] \tag{38}$$

$$c_{12} = \frac{\sigma(1+\lambda)}{l}[-n^2\left(a+l\right) + \frac{GM_1}{R_{21}^2} - \frac{GM_2}{R_{22}^3}] \tag{39}$$

$$c_{21} = \frac{1+\lambda}{\lambda l}[-n^2(\frac{1}{1+\lambda}l + a + \sigma(a+l)) -$$

$$GM_1(\frac{\rho_1}{R_{11}^3} + \frac{\rho_1 + (1+\sigma+\lambda)\frac{l}{1+\lambda}}{R_{21}^3}) - GM_2(\frac{\rho_2}{R_{12}^3} - \frac{\rho_2 + (1+\sigma+\lambda)\frac{l}{1+\lambda}}{R_{22}^3})] \tag{40}$$

$$c_{22} = \frac{1+\lambda}{\lambda l}[-an^2(1+\sigma) + n^2(1+\sigma+\lambda\sigma)\frac{l}{1+\lambda} +$$

$$GM_1\frac{\rho_1(1+\sigma) + (1+\sigma+\lambda\sigma)\frac{l}{1+\lambda}}{R_{21}^3} - GM_2\frac{\rho_2(1+\sigma) - (1+\sigma+\lambda\sigma)\frac{l}{1+\lambda}}{R_{22}^3}] \tag{41}$$

where

$$R_{11} = \rho_1 + \frac{l}{1+\lambda}, \qquad R_{12} = \rho_2 + \frac{l}{1+\lambda}, \qquad R_{21} = \rho_1 + l \;\; R_{22} = \rho_2 + l \tag{42}$$

$$\rho_1 = a + p\mu, \quad \rho_2 = a - p(1-\mu) \tag{43}$$

Taking the solution as

$$\theta_1 = A_1\cos(\omega t) \tag{44}$$

$$\theta_2 = A_2\cos(\omega t) \tag{45}$$

one can obtain a characteristic equation of the form

$$\left(c_{11} + \omega^2\right)\left(c_{22} + \omega^2\right) + c_{12}c_{21} = 0 \tag{46}$$

There are two normal modes with natural frequencies

$$\omega_{1,2}^2 = -\frac{c_{11}+c_{22}}{2} \pm \frac{1}{2}\sqrt{(c_{11}-c_{22})^2 + 4c_{12}c_{21}} \tag{47}$$

which are associated with two mode ratios

$$b_{1,2} = \frac{\theta_2}{\theta_1} = \frac{c_{22}-c_{11}}{2c_{12}} \mp \frac{1}{2c_{12}}\sqrt{(c_{11}-c_{22})^2 + 4c_{12}c_{21}} \tag{48}$$

Fig. 6 illustrates the "in phase" ($b_2 > 0$) and "out of phase" ($b_1 < 0$) motions of the double pendulum for various combinations of mass and length ratios.

a $\lambda = 1.0$, $\sigma = 1.0$

$b_1 = -1.53$ $b_2 = 0.89$

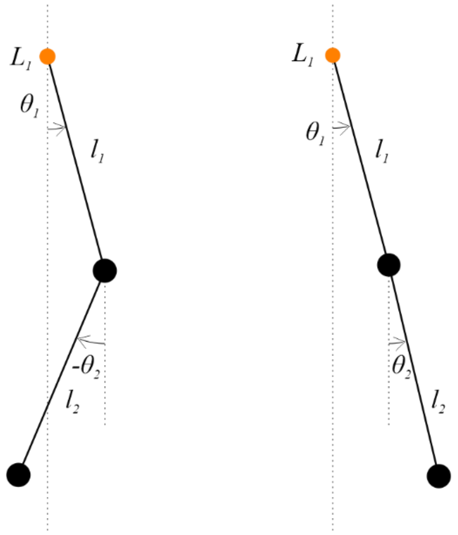

b $\lambda = 0.5$, $\sigma = 1.0$

$b_1 = -3.74$ $b_2 = 0.91$

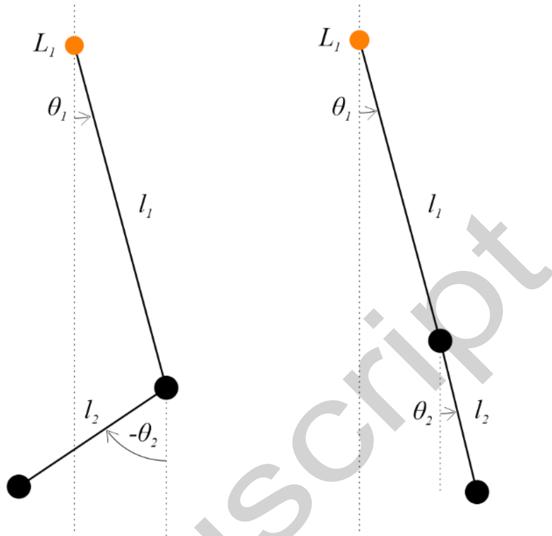

c $\lambda = 1.0$, $\sigma = 0.5$

$b_1 = -2.10$ $b_2 = 0.82$

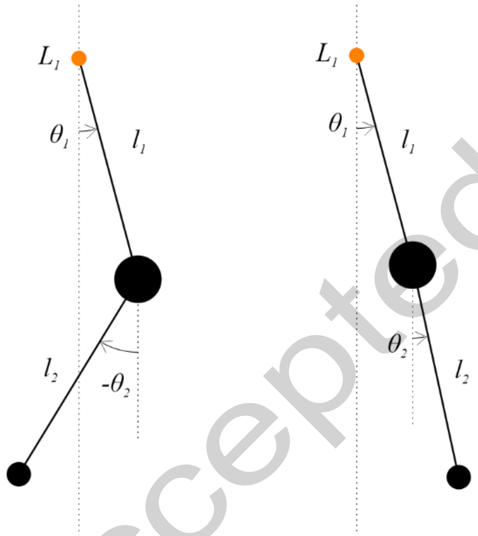

d $\lambda = 0.5$, $\sigma = 0.5$

$b_1 = -4.79$ $b_2 = 0.89$

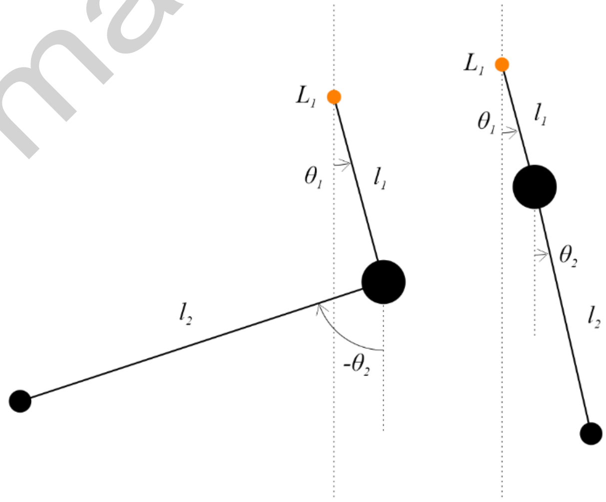

e $\lambda = 1.0$, $\sigma = 2.0$

$b_1 = -1.26$ $b_2 = 0.94$

f $\lambda = 2.0$, $\sigma = 2.0$

$b_1 = -0.59$ $b_2 = 0.95$

14

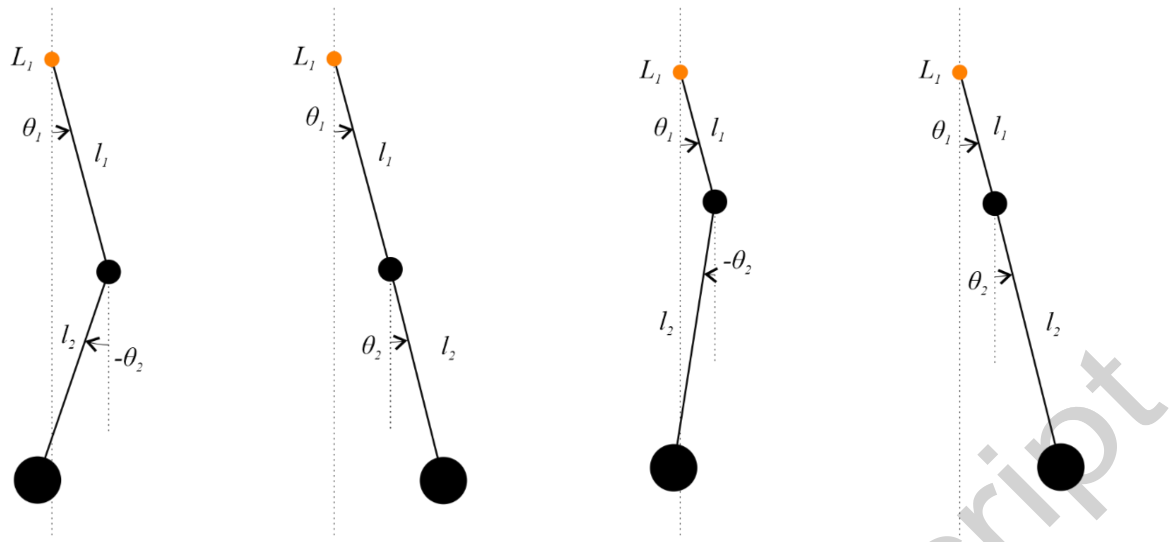

Fig. 6 The mode ratios for the double pendulum swinging toward a small primary 2

The natural frequencies (47) and the mode ratios (48) as functions of the tether length ratio $\lambda = \dfrac{l_2}{l_1}$ for various values of the pendulum mass ratios $\sigma = \dfrac{m_2}{m_1} = 0.5, 1.0, 2.0$ are shown in Figs. 7-9.

a

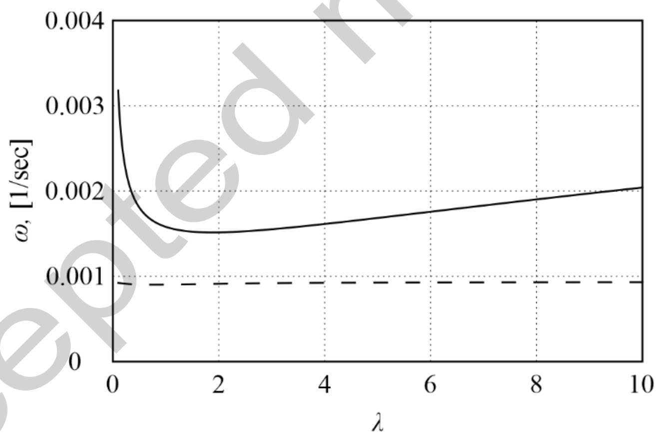

b

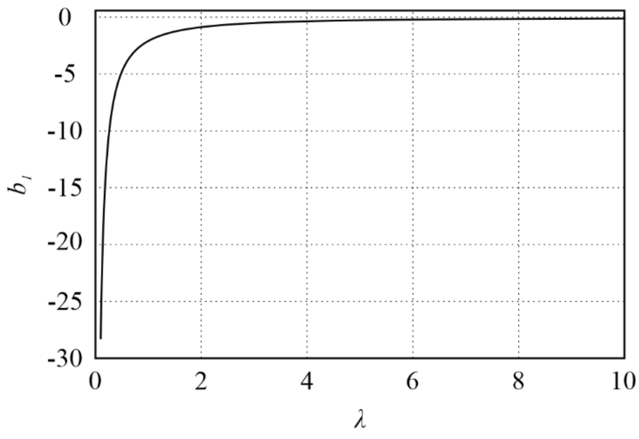

c

15

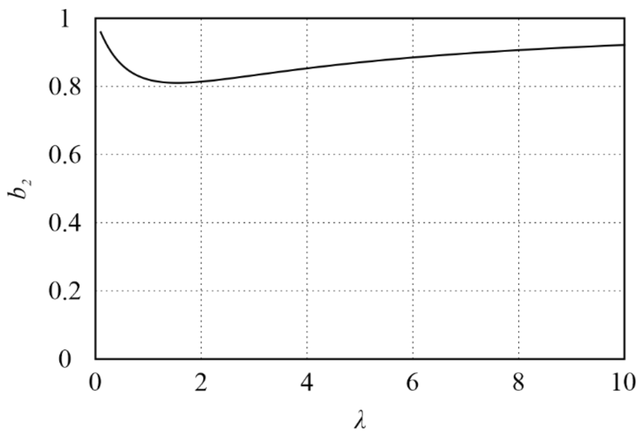

Fig. 7 a The natural frequencies ω_1 and ω_2; **b** and **c** the mode ratios b_1 and b_2 for the pendulum mass ratios $\sigma = \frac{m_2}{m_1} = 0.5$

a

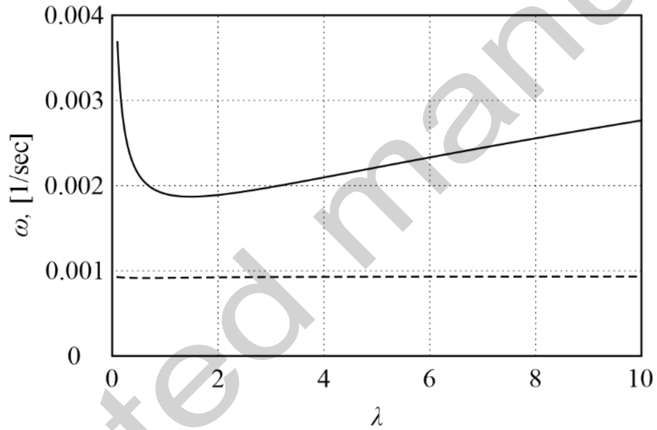

b

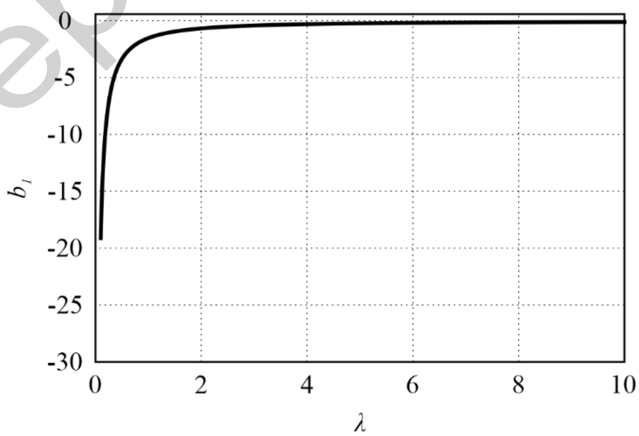

c

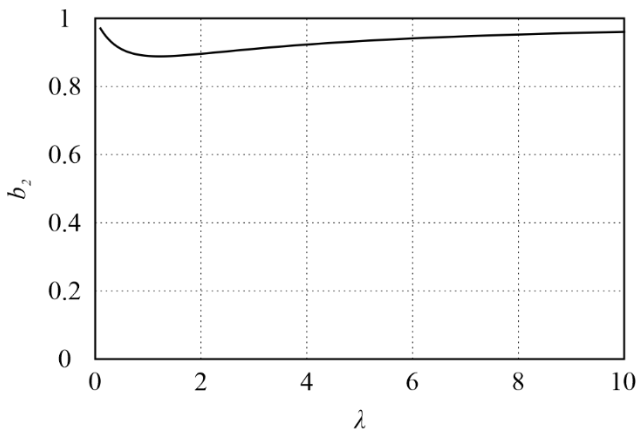

Fig. 8 a The natural frequencies ω_1 and ω_2; **b** and **c** the mode ratios b_1 and b_2 for the pendulum mass ratios $\sigma = \frac{m_2}{m_1} = 1.0$

a

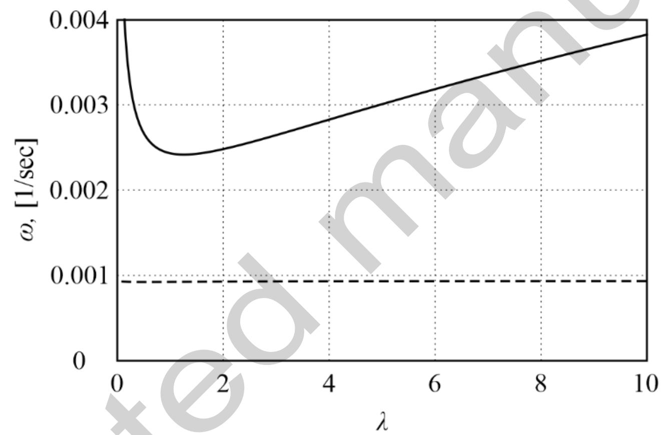

b

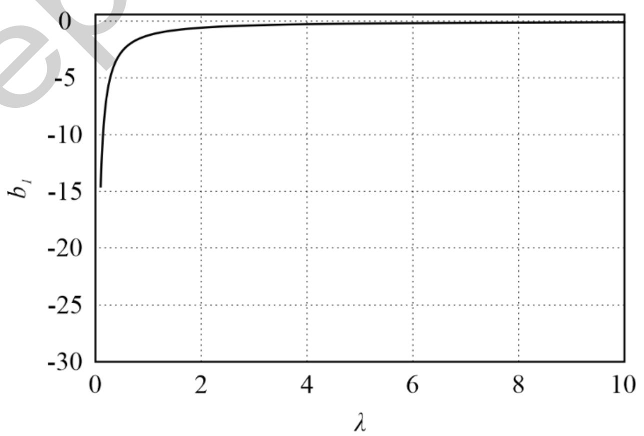

c

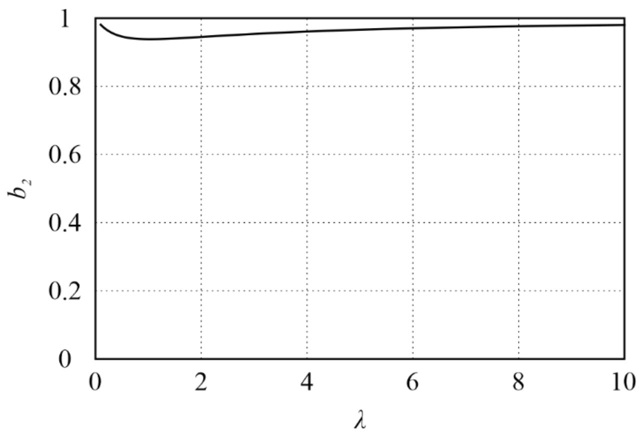

Fig. 9 a The natural frequencies ω_1 and ω_2 ; **b** and **c** the mode ratios b_1 and b_2 for the pendulum mass ratios $\sigma = \frac{m_2}{m_1} = 2.0$

The lower frequency mode b_2 is such that the two pendulums oscillate in phase while for the higher frequency b_1 mode the oscillations are out of phase. The low natural frequency ω_2 and its mode b_2 do not depend much on the ratio of the lengths λ and masses σ of the pendulums. In contrast, the mode of high natural frequency b_1 for the small ratio of lengths λ has values of the order of tens and tends to zero for large values of this ratio. The high natural frequency ω_1 has a minimum when the pendulum lengths are equal $l_2 = l_1$ ($\lambda = 1$) and increases significantly as the ratio of the lengths of the pendulums decreases and as it increases.

4.2 Small motion around equilibrium configuration $\theta_1 = \pi, \theta_2 = \pi$

By substituting the variables

$$\theta_{1,2} = \pi + \alpha_{1,2} \tag{49}$$

in the Lagrange equations (4) for small angles α_1, α_2 one can write the linear differential equations similar to Eqs. (37) as

$$\begin{pmatrix} \ddot{\alpha}_1 \\ \ddot{\alpha}_2 \end{pmatrix} = \begin{pmatrix} e_{11} & e_{12} \\ e_{21} & e_{22} \end{pmatrix} \begin{pmatrix} \alpha_1 \\ \alpha_2 \end{pmatrix} \tag{50}$$

where

$$e_{11} = \frac{1+\lambda}{l}[n^2(a + \sigma(a-l)) - GM_1(\frac{\rho_1}{R_{11}^3} + \frac{\sigma}{R_{21}^2}) + GM_2(-\frac{\rho_2}{R_{12}^3} + \frac{\sigma}{R_{22}^2})] \tag{51}$$

$$e_{12} = \frac{\sigma(1+\lambda)}{l}\left(n^2(l-a) + \frac{GM_1}{{R_{21}}^2} - \frac{GM_2}{{R_{22}}^2} \right) \tag{52}$$

$$e_{21} = \frac{1+\lambda}{\lambda l}[n^2(-a(1+\sigma)+(1+\sigma+\lambda\sigma)\frac{l}{1+\lambda})+$$

$$GM_1(\frac{\rho_1}{R_{11}^3}+\frac{\rho_1\sigma-(1+\sigma+\lambda\sigma)\frac{l}{1+\lambda}}{R_{21}^3})+GM_2(\frac{\rho_2}{R_{12}^3}-\frac{\rho_2\sigma-(1+\sigma+\lambda\sigma)\frac{l}{1+\lambda}}{R_{22}^3})] \tag{53}$$

$$e_{22} = \frac{1+\lambda}{\lambda l}[an^2((1+\sigma)-(1+\sigma+\lambda\sigma)\frac{l}{1+\lambda})-$$

$$GM_1\frac{\rho_1(1+\sigma)-(1+\sigma+\lambda\sigma)\frac{l}{1+\lambda}}{R_{21}^3}-GM_2\frac{-\rho_2\left(1+\sigma\right)+(1+\sigma+\lambda\sigma)\frac{l}{1+\lambda}}{R_{22}^3}] \tag{54}$$

where

$$R_{11} = \rho_1 - \frac{l}{1+\lambda}, \qquad R_{12} = \rho_2 - \frac{l}{1+\lambda}, \qquad R_{21} = \rho_1 - l, \quad R_{22} = \rho_2 - l \tag{55}$$

$$\rho_1 = a + p\mu, \quad \rho_2 = a - p(1-\mu) \tag{56}$$

In this case, there are two normal modes with natural frequencies

$$\Omega_{1,2}^2 = -\frac{e_{11}+e_{22}}{2} \pm \frac{1}{2}\sqrt{(e_{11}-e_{22})^2+4e_{12}e_{21}} \tag{57}$$

which are associated with two mode ratios

$$d_{1,2} = \frac{\alpha_2}{\alpha_1} = \frac{e_{22}-e_{11}}{2e_{12}} \mp \frac{1}{2e_{12}}\sqrt{(e_{11}-e_{22})^2+4e_{12}e_{21}} \tag{58}$$

Fig. 10 shows the "in phase" ($d_2 > 0$) and "out of phase" ($d_1 < 0$) motions of the double pendulum for various combinations of mass and length ratios.

a $\lambda = 1.0$, $\sigma = 1.0$

$d_1 = -1.49$ $\quad d_2 = 1.06$

b $\lambda = 0.5$, $\sigma = 1.0$

$d_1 = -3.13$ $\quad d_2 = 1.04$

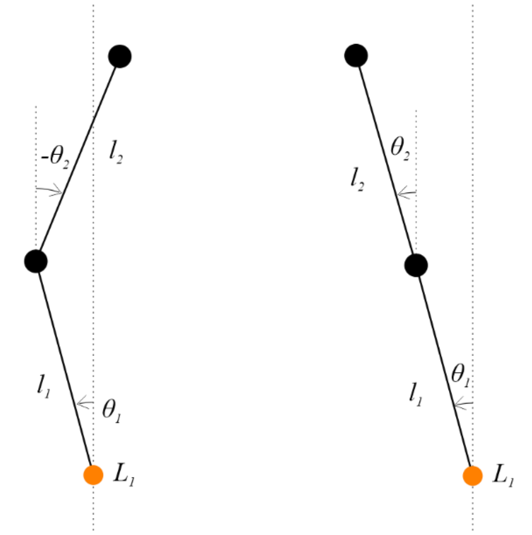

c $\lambda = 1.0$, $\sigma = 0.5$

$d_1 = -1.95 \qquad d_2 = 1.10$

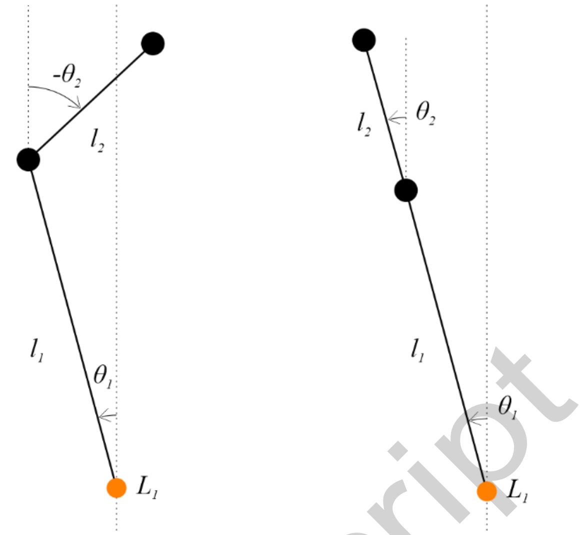

d $\lambda = 0.5$, $\sigma = 0.5$

$d_1 = -4.61 \qquad d_2 = 1.07$

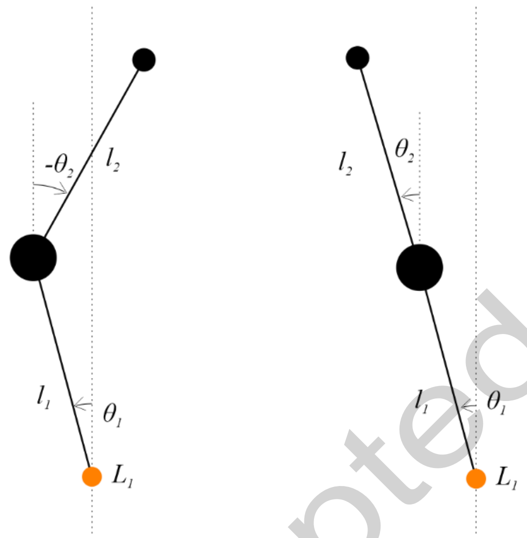

e $\lambda = 1.0$, $\sigma = 2.0$

$b_1 = -1.25 \qquad b_2 = 1.04$

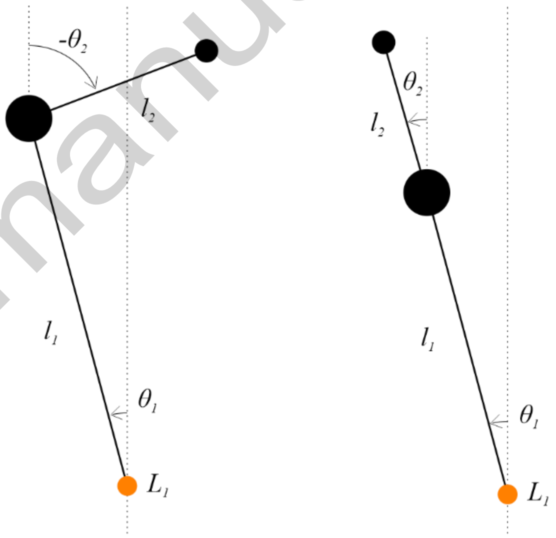

f $\lambda = 2.0$, $\sigma = 2.0$

$b_1 = -0.58 \qquad b_2 = 1.03$

20

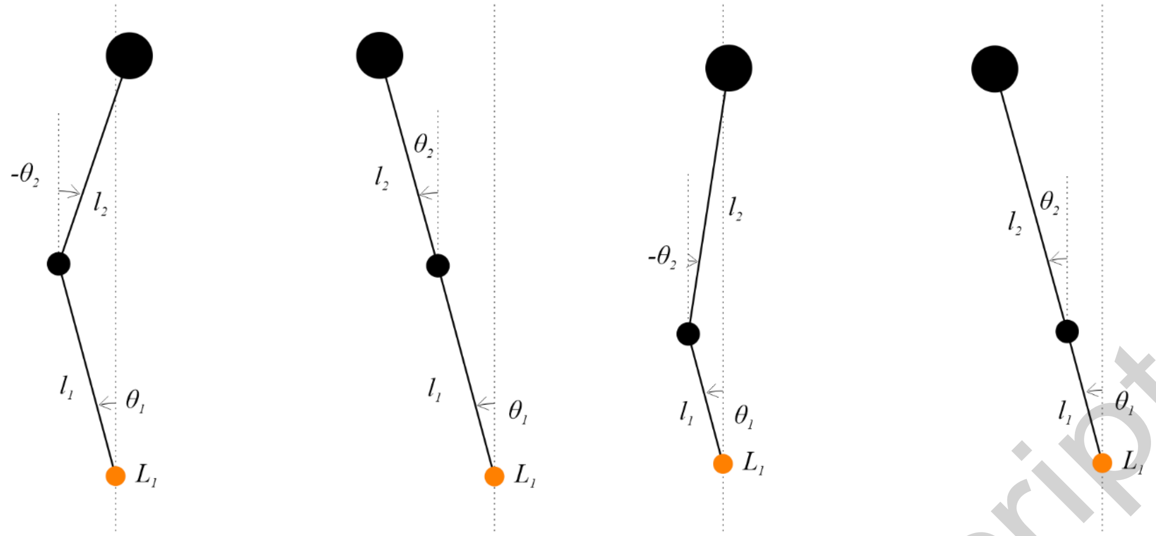

Fig. 10 The mode ratios for the double pendulum swinging toward a large primary 1

Dependences of the natural frequencies (47) and the mode ratios (48) on the relative length of the tethers $\lambda = \frac{l_2}{l_1}$ for different values of the mass ratios of the pendulums $\sigma = \frac{m_2}{m_1} = 0.5, 1.0, 2.0$ are shown in Figs. 11-13.

a

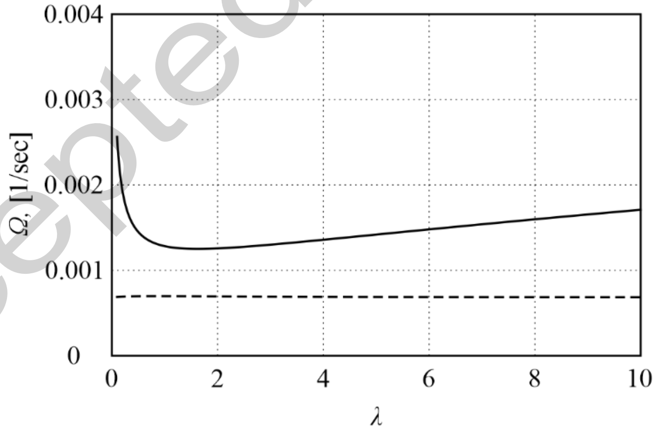

b

21

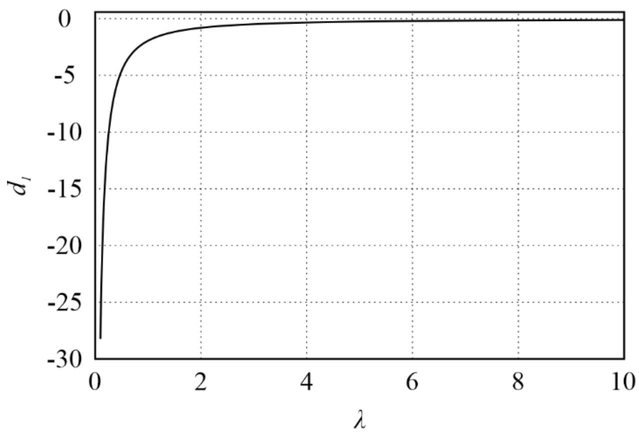

c

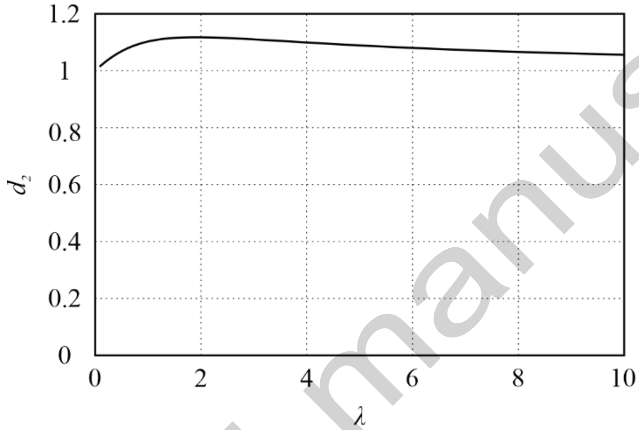

Fig. 11 a The natural frequencies Ω_1 and Ω_2; **b** and **c** the mode ratios d_1 and d_2 for the pendulum mass ratios $\sigma = \frac{m_2}{m_1} = 0.5$

a

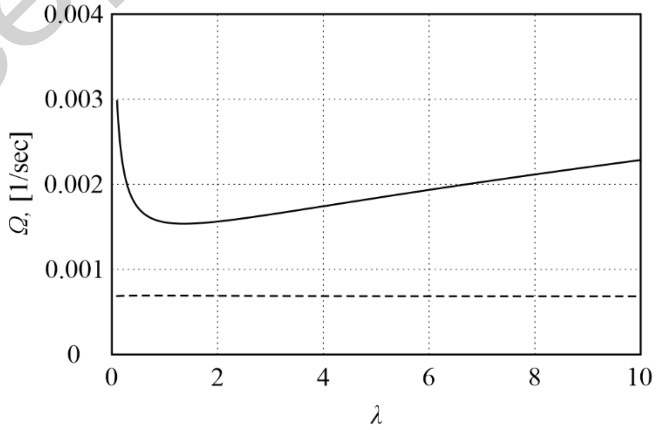

b

22

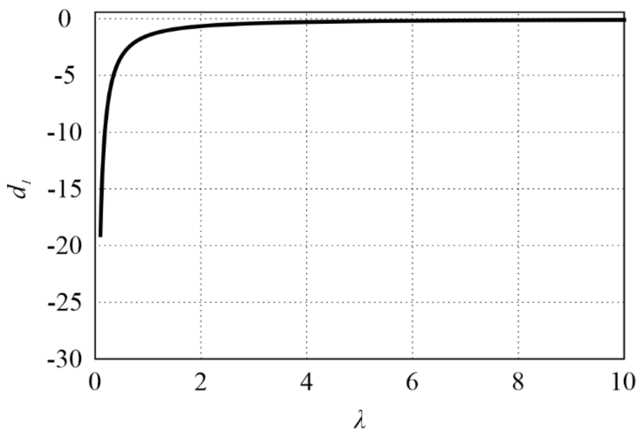

c

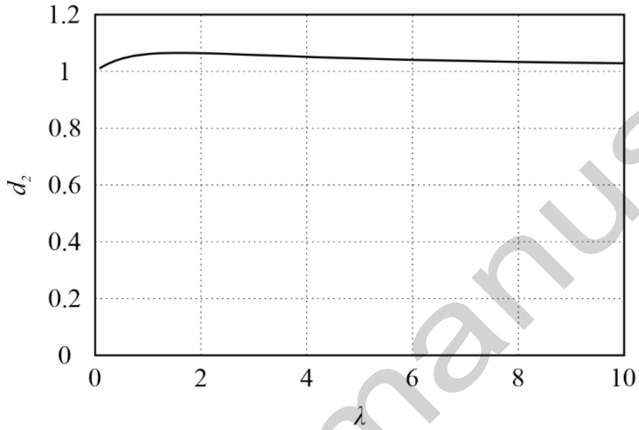

Fig. 12 a The natural frequencies Ω_1 and Ω_2 ; **b** and **c** the mode ratios d_1 and d_2 for the pendulum mass ratios $\sigma = \dfrac{m_2}{m_1} = 1.0$

a

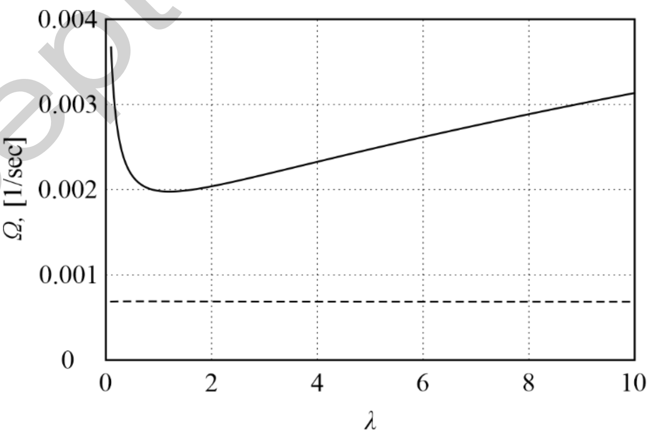

b

23

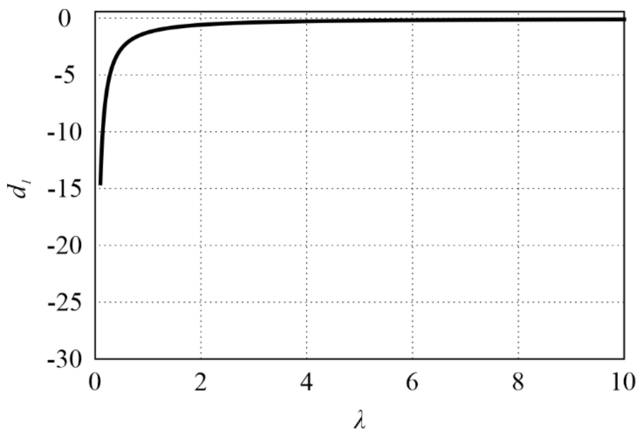

c

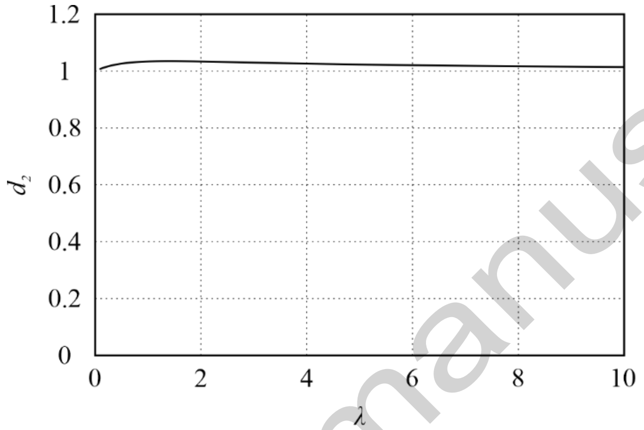

Fig. 13 a The natural frequencies Ω_1 and Ω_2; **b** and **c** the mode ratios d_1 and d_2 for the pendulum mass ratios $\sigma = \dfrac{m_2}{m_1} = 2.0$

Based on the analysis of curves shown in Figs. 4-13, it can be stated that the behavior of the double pendulums deployed in the direction of the large primary 1 or in the direction of the small primary 2 is very similar.

5 Conclusions

The main analytical results of the paper are summarized as follows:

1. In the framework of the restricted circular three-body problem, the equations of motion of a double pendulum fixed at the L1 libration point are obtained. The possible configurations of the equilibrium positions, which depend on the ratios of the masses and lengths of the single pendulums constituting the double pendulum, are constructed.

24

2. Using Sylvester's criterion, the stability of two equilibrium positions is proved for the cases when the double pendulum is oriented toward the primary 2 $\theta_1 = 0, \theta_2 = 0$ and to the primary 1 $\theta_1 = \pi, \theta_2 = \pi$.

3. Small motions about equilibrium configurations $\theta_1 = 0, \theta_2 = 0$ and $\theta_1 = \pi, \theta_2 = \pi$ are studied.

The natural frequencies and mode ratios are obtained analytically and their dependence on the mass and length ratios of the pendulums is analyzed.

The main conclusions about the feasibility of the space elevator fixed at the L1 libration point, designed on the basis of the research conducted, are as follows:

1. The stability of the vertical equilibrium positions makes it possible to construct a space elevator from the L1 libration point to primary 2 (distance from the L1 point to the surface of Phobos ~3.4 km), or to primary 1 (distance from the L1 point to the surface of Mars ~7800 km).

2. An important result is the fact that the natural frequencies and mode ratios are very close for the cases of a space elevator deployment both in the direction of primary 1 and in the direction of primary 2. This opens the possibility of building a two-part space elevator from primary 1 to primary 2, e.g. from Mars to Phobos.

3. The obtained natural frequencies and mode ratios allow to predict in advance the possible motions of a space elevator under small perturbations relative to the stable equilibrium position.

Acknowledgements I would like to thank Dr. Alexander Ledkov for helpful discussions of the results.

Data availability The datasets generated during and/oranalyzed during the current study are available from the corresponding author on reasonable request.

Declarations

Conflict of interest The author declares that he has no conflict of interest.

References

1. Beletsky, V.V., Levin, E.M.: Dynamics of space tether systems. Univelt Incorporated, San Diego (1993)

2. Levin, E.M.: Dynamic Analysis of Space Tether Missions. Univelt Incorporated, San Diego (2007)

25

3. Troger, H., Alpatov, A.P., Beletsky, V.V., Dranovskii, V.I.,Khoroshilov, V.S., Pirozhenko, A.V., Zakrzhevskii, A.E.: Dynamics of Tethered Space Systems. CRC Press, New York (2010)

4. Aslanov, V.S., Ledkov, A.S.: Dynamics of Tethered Satellite Systems. Woodhead Publishing, Cambridge (2012)

5. Williams, P., Hyslop, A., Stelzer, M., and Kruijff, M. YES2 Optimal Trajectories in Presence of Eccentricity and Aerodynamic Drag. Acta Astronautica, 64(7), 745–769 (2009). doi:10.1016/j.actaastro.2008.11.007

6. Williams, P., Blanksby, C., and Trivailo, P. Tethered Planetary Capture Maneuvers. Journal of Spacecraft and Rockets, 41(4), 603–613 (2004). doi:10.2514/1.1024

7. Jung, W., Mazzoleni, A.P. & Chung, J. Nonlinear dynamic analysis of a three-body tethered satellite system with deployment/retrieval. Nonlinear Dyn 82, 1127–1144 (2015). https://doi.org/10.1007/s11071-015-2221-z

8. Huang, P., Zhang, F., Chen, L. et al. A review of space tether in new applications. Nonlinear Dyn 94, 1–19 (2018). https://doi.org/10.1007/s11071-018-4389-5

9. Yu, B.S., Xu, S.D. & Jin, D.P. Chaos in a tethered satellite system induced by atmospheric drag and Earth's oblateness. Nonlinear Dyn 101, 1233–1244 (2020). https://doi.org/10.1007/s11071-020-05844-8

10. Ledkov, A., Aslanov, V. Evolution of space tethered system's orbit during space debris towing taking into account the atmosphere influence. Nonlinear Dyn 96, 2211–2223 (2019). https://doi.org/10.1007/s11071-019-04918-6

11. Kumar, K. D., and Kumar, K. Attitude Maneuver of Dual Tethered Satellite Platforms Through Tether Offset Change. Journal of Spacecraft and Rockets, 38, 2, , 237–242 (2001). https://doi.org/10.2514/2.3676

12. Kumar, K., Yasaka, T.: Rotation formation flying of three satellites using tethers. Journal of Spacecraft and Rockets. 41(6), 973–85 (2004). https://doi.org/10.2514/1.14251

13. Cartmell, M.P., McKenzie, D.J. A review of space tether research. Prog. Aerosp. Sci. 44(1), 1–21 (2008). https://doi.org/10.1016/j.paerosci.2007.08.002

14. Mashayekhi, M. J., & Misra, A. K. Optimization of tether-assisted asteroid deflection. Journal of Guidance, Control, and Dynamics, 37(3), 898-906 (2014). https://doi.org/10.2514/1.60176

15. Kempton, K., Pearson, J., Levin, E., Carroll, J., & Amzajerdian, F., "Phase 1 Study for the Phobos L1 Operational Tether Experiment (PHLOTE)," End Report, NASA, 2018, pp.1-91. https://ntrs.nasa.gov/search.jsp?R=20190000916.

26

16. Sun, G., Zhu, Z. Fractional-order tension control law for deployment of space tether system. Journal of Guidance, Control, and Dynamics. 37(6), 2057–167 (2014). https://doi.org/10.2514/1.G000496

17. Aslanov, V.S.: Prospects of a tether system deployed at the L1 libration point. Nonlinear Dyn. 106, 2021–2033 (2021).

18. https://doi.org/10.1007/s11071-021-06884-4Misra, A.K., Amier, Z., Modi, V.J.: Attitude dynamics of three-body tethered systems. Acta Astronaut. 17(10), 1059–1068 (1988). https://doi.org/10.1016/0094-5765(88)90189-0

19. Kumar, K., Kumart, R., Misra, A.K.: Effects of deploymentrates and librations on tethered payload raising. J. Guid. Control Dyn. 15(5), 1230–1235 (1992)

20. Woo, P., Misra, A.K.: Dynamics of a partial space elevator with multiple climbers. Acta Astronaut. 67(7–8), 753–763 (2010)

21. Shi, G., Zhu, Z. & Zhu, Z.H. Libration suppression of tethered space system with a moving climber in circular orbit. Nonlinear Dyn 91, 923–937 (2018). https://doi.org/10.1007/s11071-017-3919-x

22. Aslanov, V.S., Ledkov, A.S., Misra, A.K., Guerman, A.D. Dynamics of space elevator after tether rupture. Journal of Guidance, Control, and Dynamics, 36(4), 986–992 (2013). https://doi.org/10.2514/1.59378

23. Samaranayake, S., Bajaj, A.K. Bifurcations in the dynamics of an orthogonal double pendulum. Nonlinear Dyn 4, 605–633 (1993). https://doi.org/10.1007/BF00162234

24. Singh, S., Mukherjee, S., Sanghi, S. Study of a self-impacting double pendulum. Journal of sound and vibration, 318 (4-5), 1180-1196 (2008). doi:10.1016/j.jsv.2008.05.001.

25. Roy, J., Mallik, A.K., Bhattacharjee, J.K. Role of initial conditions in the dynamics of a double pendulum at low energies. Nonlinear Dyn 73, 993–1004 (2013). https://doi.org/10.1007/s11071-013-0848-1

26. Kovacic, I., Zukovic, M. & Radomirovic, D. Normal modes of a double pendulum at low energy levels. Nonlinear Dyn 99, 1893–1908 (2020). https://doi.org/10.1007/s11071-019-05424-5

27. Puzyrov, V., Awrejcewicz, J., Losyeva, N., Savchenko, N. (2022). On the stability of the equilibrium of the double pendulum with follower force: Some new results. Journal of Sound and Vibration, 523, 116699. https://doi.org/10.1016/j.jsv.2021.116699

28. Puzyrov, V., Awrejcewicz, J. Asymptotical stability of the motion of mechanical systems with partial energy dissipation. Nonlinear Dyn 91, 329–341 (2018). https://doi.org/10.1007/s11071-017-3872-8

27

29. Dudkowski, D., Wojewoda, J., Czołczyński, K. et al. Is it really chaos? The complexity of transient dynamics of double pendula. Nonlinear Dyn 102, 759–770 (2020). https://doi.org/10.1007/s11071-020-05697-1

30. 30. Zhang, M., Ma, X., Chai, H. et al. A novel online motion planning method for double-pendulum overhead cranes. Nonlinear Dyn 85, 1079–1090 (2016). https://doi.org/10.1007/s11071-016-2745-x

31. Kovacic, I., & Radomirovic, D. (2017). Mechanical vibration: Fundamentals with solved examples. John Wiley & Sons.

32. He, J., Cui, L., Sun, J. et al. Chaotic dynamics analysis of double inverted pendulum with large swing angle based on Hamiltonian function. Nonlinear Dyn 108, 4373–4384 (2022). https://doi.org/10.1007/s11071-022-07455-x

33. Kaheman, K., Bramburger, J.J., Kutz, J.N. et al. Saddle transport and chaos in the double pendulum. Nonlinear Dyn 111, 7199–7233 (2023). https://doi.org/10.1007/s11071-023-08232-0

34. Guo, Q., Chai, L. & Liu, H. Anti-swing sliding mode control of three-dimensional double pendulum overhead cranes based on extended state observer. Nonlinear Dyn 111, 391–410 (2023). https://doi.org/10.1007/s11071-022-07859-9

35. Lyu, W., Zhang, L., Jiang, H. et al. Slow–fast dynamics in a perturbation model of double pendulum system with singularity of triple zero eigenvalues. Nonlinear Dyn 111, 3239–3252 (2023). https://doi.org/10.1007/s11071-022-08020-2

36. Jaafar, H. I., Mohamed, Z., Shamsudin, M. A., Subha, N. M., Ramli, L., & Abdullahi, A. M., Model reference command shaping for vibration control of multimode flexible systems with application to a double-pendulum overhead crane. Mechanical Systems and Signal Processing, 115, 677-695 (2019). https://doi.org/10.1016/j.ymssp.2018.06.005

37. Kumar, R., Gupta, S., & Ali, S. F., Energy harvesting from chaos in base excited double pendulum. Mechanical Systems and Signal Processing, 124, 49-64 (2019). https://doi.org/10.1016/j.ymssp.2019.01.037

38. Dudkowski, D., Wojewoda, J., Czołczyński, K. et al. Is it really chaos? The complexity of transient dynamics of double pendula. Nonlinear Dyn 102, 759–770 (2020). https://doi.org/10.1007/s11071-020-05697-1

39. Szebehely, V.: The Restricted Problem of Three Bodies, Academic Press Inc., New York (1967)

40. Hertz, H.: The principles of mechanics presented in a new form. Macmillian and Company, Limited (1899)

28

41. Routh, E. J.: A treatise on the stability of a given state of motion, particularly steady motion: being the essay to which the Adams prize was adjudged in 1877, in the University of Cambridge. Macmillan and Company (1877).

42. Merkin, D. R.: Introduction to the Theory of Stability (Vol. 24). pp.76 Springer Science & Business Media (1996)

43. Wolfram, S.: The Mathematica Book, fifth ed., Cambridge Univ. Press, Cambridge, England, U.K., 2003

29